

Carboxylesterase 2 induces mitochondrial dysfunction via disrupting lipid homeostasis in oral squamous cell carcinoma



Xijuan Chen¹, Qin Liu¹, Yingyao Chen¹, Lixuan Wang, Rongchun Yang, Weilin Zhang, Xue Pan, Siyuan Zhang, Chuwen Chen, Tong Wu, Juan Xia, Bin Cheng^{***}, Xiaobing Chen^{**}, Xianyue Ren^{*}

ABSTRACT

Objective: Oral squamous cell carcinoma (OSCC) is characterized by high recurrence and metastasis and places a heavy burden on societies worldwide. Cancer cells thrive in a changing microenvironment by reprogramming lipidomic metabolic processes to provide nutrients and energy, activate oncogenic signaling pathways, and manage redox homeostasis to avoid lipotoxicity. The mechanism by which OSCC cells maintain lipid homeostasis during malignant progression is unclear.

Methods: The altered expression of fatty acid (FA) metabolism genes in OSCC, compared with that in normal tissues, and in OSCC patients with or without recurrence or metastasis were determined using public data from the TCGA and GEO databases. Immunohistochemistry was performed to examine the carboxylesterase 2 (CES2) protein level in our own cohort. CCK-8 and Transwell assays and an *in vivo* xenograft model were used to evaluate the biological functions of CES2. Mass spectrometry and RNA sequencing were performed to determine the lipidome and transcriptome alterations induced by CES2. Mitochondrial mass, mtDNA content, mitochondrial membrane potential, ROS levels, and oxygen consumption and apoptosis rates were evaluated to determine the effects of CES2 on mitochondrial function in OSCC.

Results: CES2 was downregulated in OSCC patients, especially those with recurrence or metastasis. CES2^{high} OSCC patients showed better overall survival than CES2^{low} OSCC patients. Restoring CES2 expression reduced OSCC cell viability and suppressed their migration and invasion *in vitro*, and it inhibited OSCC tumor growth *in vivo*. CES2 reprogrammed lipid metabolism in OSCC cells by hydrolyzing neutral lipid diacylglycerols (DGs) to release free fatty acids and reduce the membrane structure lipid phospholipids (PLs) synthesis. Free FAs were converted to acyl-carnitines (CARs) and transferred to mitochondria for oxidation, which induced reactive oxygen species (ROS) accumulation, mitochondrial damage, and apoptosis activation. Furthermore, the reduction in signaling lipids, e.g., DGs, PLs and substrates, suppressed PI3K/AKT/MYC signaling pathways. Restoring MYC rescued the diminished cell viability, suppressed migratory and invasive abilities, damaged mitochondria and reduced apoptosis rate induced by CES2.

Conclusions: We demonstrated that CES2 downregulation plays an important role in OSCC by maintaining lipid homeostasis and reducing lipotoxicity during tumor progression and may provide a potential therapeutic target for OSCC.

© 2022 The Author(s). Published by Elsevier GmbH. This is an open access article under the CC BY-NC-ND license (<http://creativecommons.org/licenses/by-nc-nd/4.0/>).

Keywords Oral squamous cell carcinoma; CES2; Diacylglycerols; Lipotoxicity; Mitochondrial damage

1. INTRODUCTION

With approximately 350,000 new cases diagnosed and 170,000 deaths per year worldwide, oral squamous cell carcinoma (OSCC) remains a major health issue and societal burden. Unfortunately, the five-year survival rate of OSCC patients has remained relatively unchanged for the last several decades. Recurrence and metastasis are the main treatment failure events of OSCC patients [1]. Understanding

the molecular mechanism that drives OSCC progression remains the primary mission of current research.

Lipids, playing classical roles in membrane construction, energy provision, redox homeostasis balance, intracellular messenger generation and protein modification, are central to cancer growth, survival, and metastasis [2,3]. For example, phospholipids (PLs), together with cholesterol and sphingolipids, are the major components of biological membranes. Signaling intermediates, such as diacylglycerols (DGs),

Hospital of Stomatology, Guangdong Provincial Key Laboratory of Stomatology, Sun Yat-sen University, Guangzhou 510055, Guangdong, People's Republic of China

¹ Xijuan Chen, Qin Liu and Yingyao Chen contributed equally to this article.

*Corresponding author. Guangzhou 510080, Guangdong, China. E-mail: renxy7@mail.sysu.edu.cn (X. Ren).

**Corresponding author. E-mail: chenxb7@mail.sysu.edu.cn (X. Chen).

***Corresponding author. E-mail: chengbin@mail.sysu.edu.cn (B. Cheng).

Received June 23, 2022 • Revision received August 31, 2022 • Accepted September 9, 2022 • Available online 14 September 2022

<https://doi.org/10.1016/j.molmet.2022.101600>

Abbreviations			
OSCC	oral squamous cell carcinoma	PI	phosphatidylinositol
CES	carboxylesterases	PA	phosphatidic acid
TCGA	The Cancer Genome Atlas	LPC	lysophosphatidylcholine
GEO	Gene Expression Omnibus	LPE	lysophosphatidylethanolamine
ROC	receiver operating characteristic	FA	fatty acid
OS	overall survival	CE	cholesterol
CCK8	Cell Counting Kit-8	SM	sphingomyelin
IHC	Immunohistochemistry	CER	ceramides
TG	triacylglycerol	CAR	acyl-carnitines
DG	diacylglycerol	FAO	fatty acid oxidation
MG	monoglyceride	ROS	reactive oxygen species
PL	Phospholipid	NAFLD	nonalcoholic fatty liver disease
PC	phosphatidylcholine	PDAC	pancreatic ductal adenocarcinoma
PE	phosphatidylethanolamine	ER	endoplasmic reticulum
PS	phosphatidylserine	OCR	oxygen consumption rate
		ECAR	extracellular acidification rate
		DGL	diacylglycerol lipase

phosphatidylinositols (PIs), phosphatides, ceramides, sphingosines and oxylipins, play important roles in facilitating mitogenic and oncogenic signaling. Fatty acids (FAs) are aliphatic hydrocarbons with polar carboxylic headgroups and are essential to build blocks of complex lipids, which are the major source of mitochondrial oxidative metabolism and NADH synthesis. Despite their essential roles in cellular fundamental physiological functions, FA levels in excess are very detrimental because they lead to lipotoxicity and even to cellular dysfunction and cell death [4,5]. Reprogramming of lipid metabolism, a recognized hallmark of cancers [6], is comparatively less well characterized than the metabolism of other nutrients in OSCC. The mechanisms by which OSCC cells maintain FA pool homeostasis to support tumor progression and prevent lipotoxicity are unclear.

CES2 (carboxylesterase 2), a major CES isoform, preferentially hydrolyzes esters with a relatively small acyl group and a large alcohol group. It has been extensively studied for its ability to metabolize anticancer drugs, such as irinotecan (CPT-11), capecitabine, procaine and flutamide. Recently, the hydrolytic activity of CES2 of endogenous lipids has attracted attention [7–9]. CES2 has been verified to be a neutral lipid lipase that can hydrolyze triacylglycerols (TGs), diacylglycerols (DGs) and monoglycerides (MGs). Aberrant expression of CES2 has been correlated with many metabolic diseases, such as nonalcoholic fatty liver disease (NAFLD) [8], obesity [9] and cancers. However, it remains unclear how CES2 participates in lipid metabolism reprogramming in cancer cells. The roles played by CESs in OSCC lipid homeostasis and tumorigenesis are unknown and need to be elucidated.

In this study, we comprehensively characterized the different expression patterns of FA metabolism genes in normal epithelial tissues and compared the patterns found for nonrecurring OSCC tissues and non-metastatic tissues with those found for tissues with OSCC recurrence or metastasis. We aimed to identify the key molecular event involved in maintaining FA pool homeostasis during OSCC progression. The lipase CES2 gene was downregulated in advanced OSCC and acted as a tumor suppressor, which might uncover the previously unrecognized molecular mechanism regulating lipid homeostasis and provide novel insight into clinical therapy strategy development for OSCC patients.

2. MATERIALS AND METHODS

2.1. Clinical specimens

This research was authorized by the Institutional Ethical Review Boards of Hospital of Stomatology, Sun Yat-sen University. Five normal oral

epithelial tissues and fifteen formalin-fixed paraffin-embedded OSCC tissues were collected from patients with written informed consents who received no anti-tumor therapy before biopsy collection. All samples were stained by hematoxylin and eosin (H&E) and validated by two authoritative pathologists. The mRNA expression profiles and patients' clinical profiles in head and neck squamous cell carcinoma (HNSC) were downloaded from the TCGA and GEO databases (GSE30784, GSE25099, GSE25104, GSE31056 and GSE37991). The CES2 methylation levels were calculated using the Human Methylation 450K BeadChip (Illumina) from TCGA, GSE75537 and GSE87053. The clinical information of the patients is shown in Table S1.

2.2. Immunohistochemistry (IHC)

IHC was performed with OSCC formalin-fixed, paraffin-embedded (FFPE) sections as we have previously described [10]. Briefly, the tissues were deparaffinized using xylene and rehydrated with gradient concentrations of alcohol. After blocking the endogenous peroxidase activity by 3% H₂O₂, the tissues were subjected to citrate-mediated high-temperature antigen retrieval. Nonspecific binding was blocked in the tissues, and the tissues were incubated with a primary antibody (anti-CES2, 1:100, 15378-1-AP, Proteintech) at 4 °C overnight. All sections were scored by two experienced pathologists. The expression level was calculated using the following equation: staining index = staining intensity × percentage of positive cells. The staining intensity was defined as follows: 0, no staining; 1, weak, light yellow; 2, moderate, yellow-brown; and 3, strong, brown. The proportion of positive cells was defined as follows: 1, <10%; 2, 10–35%; 3, 35–70%; 4, >70%.

2.3. Cell culture

Human OSCC cell lines (CAL27, CAL33, UM1, HSC3 and HSC6), oral keratinocyte HOK and 293FT cell lines were maintained in our own laboratory (Guangdong Provincial Key Laboratory of Stomatology, Sun Yat-sen University, China) [11–13]. The CAL27 and 293FT cells were purchased from American Type Culture Collection (ATCC). The CAL33 cells was purchased from Deutsche Sammlung von Mikroorganismen und Zellkulturen (DSMZ). The HSC3 cells were obtained from the Japanese Collection of Research Bioresources Cell Bank (JCRB). The UM1 and HSC6 cells were generously provided by Prof. Huang Hongzhang (Sun Yat-sen University, China) and Prof. J Silvio Gutkind (National Institutes of Health, USA), respectively. The HOK cells were purchased from ScienCell Research Laboratories. All the cell lines were

authenticated before use. The CAL27, CAL33, HSC3, HSC6 and 293FT cells were cultured in Dulbecco's modified Eagle's medium (DMEM) (Invitrogen) supplemented with 10% fetal bovine serum (FBS) (Gibco). The UM1 cells were grown in DMEM/F-12 supplemented with 10% FBS. The HOK cells were cultured on PLL-coated dishes in Keratinocyte-SFM (Gibco) supplemented with penicillin (100 U/mL).

2.4. 5-aza-2'-deoxy-cytidine (5-Aza) treatment

For the methyltransferase inhibitor 5-Aza (A3656, Sigma-Aldrich, USA) treatment, 1.5×10^5 OSCC cells were seeded on 60 mm culture dishes. After 24 h of growth, the cells were treated with DMSO or 5-Aza (2.5 μ m) by replacing the drug every day for 3 days. Then, cells were harvested for RNA extraction.

2.5. Plasmid construction and transfection

The pSin-EF2-puro-Vector, pSin-EF2-puro-CES2-HA, pLVX-IRES-Neo, and pLVX-IRES-Neo-MYC-FLAG plasmids were obtained from Long Bioscience (China). The full-length CDS of human CES2 (NM_001365405.1) was cloned into a pSin-EF2-puromycin plasmid between the SpeI and NdeI restriction sites. The full-length CDS of human MYC (NM_001354870.1) was cloned into a pLVX-IRES-Neo plasmid between the EcoRI and BamHI restriction sites.

The pSin-EF2-empty vector or pSin-EF2-CES2 plasmids and the lentivirus packaging plasmids (pMD2.G and psPAX2) were co-transfected into 293FT cells using the calcium phosphate method, as previously described [14]. Lentivirus particles were harvested and infected into the CAL33 and UM1 cells. The vector or CES2 stably transfected cells were selected using puromycin (0.5 μ g/ml) (Sigma). Western blot assays were performed to measure the effects of over-expressed genes.

For transient transfection, Lipofectamine 3000 reagent (Invitrogen) was used according to the manufacturer's instructions. After transfection with siRNA oligonucleotides (100 nM) or plasmids (2 μ g) for 36–48 h, the cells were collected for further study.

2.6. RNA and DNA extraction

For total RNA extraction, TRIzol reagent (Invitrogen) was used to lyse OSCC cells while maintaining RNA integrity. Then, chloroform was added to the mixture. After centrifugation, RNA was precipitated with isopropanol, washed with ethanol and resolved into RNase-free H₂O. The TIANamp Genomic DNA Kit (Tiagen) was used to isolate the genomic DNA from OSCC cells according to the manufacturer's instructions. Nanodrop One spectrophotometer (Thermo Scientific) and Agilent 2100 bioanalyzer (Agilent) were used to quantify and qualify the RNA and DNA. RNA and DNA were stored at -20 °C until use.

2.7. RNA sequencing (RNA-seq) and bioinformatics analysis

Before sequencing, an RNA Clean XP Kit (Beckman Coulter) and RNase-Free DNase Set (QIAGEN) were used to purify the total RNA. Random primers (Promega) and reverse transcriptase (Promega) were applied to synthesize complementary DNA. RNA-seq was conducted by the Longsee Medical Corporation (Guangzhou, China) using an HiSeq X ten platform (Illumina). The human reference genome sequence (hg38) assembly generated with HISAT2 (Version 2.1.0) was used to map the RNA-seq reads. The gene expression levels were quantified with the R/Bioconductor package edgeR. The differential gene expression level was defined as fold change >1.5 and p value < 0.05 . Gene Set Enrichment Analysis (GSEA) and GO (Gene Ontology) analysis were performed to explore the biological function of OSCC cells with CES2 overexpression and compare it to that of cells with empty vector overexpression.

2.8. Quantitative real-time PCR assay

The quantitative real-time PCR (qPCR) was performed to measure the mRNA level of CES2 and the mitochondrial DNA content. The Light-Cycler 96 system (Roche) was used to conduct the SYBR Green-based (Invitrogen) qPCR analysis. ACTB was considered as an endogenous control for CES2. B2M was a set of nuclear-specific gene. The comparative threshold cycle equation ($2^{-\Delta\Delta CT}$) was performed to calculate the relative expression levels. The relative mitochondrial DNA content was calculated as: $\Delta CT = CT^{mt-Mito} - CT^{B2M}$. The following primer sequences were used: CES2 (forward): 5'-CTAGGTCCGCTGC-GATTG-3'; CES2 (reverse): 5'-TGAGGTCTGTAGACACATGG-3'; ACTB (forward): 5'-TTCTACAATGAGCTGCGTGTG-3'; ACTB (reverse): 5'-GGTCTCAAACATGATCTGGGTC-3'; mt-Mito (forward): 5'-CACTTTCCA-CACAGACATCA-3'; mt-Mito (reverse): 5'-TGGTTAGGCTGGTGTAGGG-3'; B2M (forward): 5'-TGTTCTGCTGGGTAGCTCT-3'; B2M (reverse): 5'-CCTCCATGATG CTGCTTACA-3'.

2.9. Western blot assay

The target gene protein levels were determined by western blot assay as previously described [10]. Briefly, total proteins were extracted using radioimmunoprecipitation assay buffer (RIPA) supplemented with protease inhibitor cocktail (Roche). Sodium dodecyl sulfate–polyacrylamide gel electrophoresis (10%) was performed to separate the proteins in the samples. Next, the separated proteins were transferred to the polyvinylidene fluoride membranes (Millipore). After blocking in 5% non-fat milk, the membranes were incubated with primary antibodies at 4 °C overnight, followed by incubation with species-matched secondary antibodies. Finally, enhanced chemiluminescence (Thermo) was applied to test the antigen–antibody reaction, and β -actin was used as a loading control. The following antibodies were used in this study: anti-CES2 (1:1000, Proteintech, 15378-1-AP), anti-Flag (1:1000, Sigma, F1804), anti-cleaved-PARP (1:1000, Cell signaling technology, 5625S), anti-cleaved-caspase 3 (1:1000, Cell signaling technology, 9664S), anti-Cytochrome C (1:5000, Proteintech, 66264-1-IG), anti-p-mTOR ser2448 (1:1000, Cell signaling technology, 5536T), anti-mTOR (1:1000, Cell signaling technology, 2983T), anti-p-AKT thr308 (1:1000, Cell signaling technology, 13038T), anti-p-AKT ser473 (1:1000, Cell signaling technology, 4060T), anti-AKT (1:1000, Proteintech, 10176-2-AP), anti-p-GSK3 β ser9 (1:1000, Cell signaling technology, 5558T), anti-GSK3 β (1:1000, Proteintech, 22104-1-AP), anti-MYC (1:2000, Proteintech, 10828-1-AP), anti- β -actin (1:1000, Proteintech, 66009-1-Ig), anti-rabbit IgG (1:5000, Cell signaling technology, 7074S), anti-mouse IgG (1:5000, Cell signaling technology, 7076S).

2.10. CCK-8 assay

A total of 1×10^3 cells/well were seeded in 96-well plates and incubated for the indicated times (1, 2, 3, 4, and 5 days). Then, 100 μ l of serum-free medium supplemented with 10 μ l of CCK-8 reagent (Sigma) was added to each well and incubated for 2 h. Cell viability was determined on the basis of absorbance measured at 450 nm with a spectrophotometric plate reader (BioTek).

2.11. Transwell assays

A total of 1×10^5 cells suspended in serum-free medium were added to the upper Transwell chambers (Invitrogen) pre-coated without (for the migration assay) or with Matrigel (for the invasion assay) (Invitrogen). Medium containing 10% FBS was added to the lower Transwell chambers. After growing for 18 h (migration assay) or 24 h (invasion assay), the cells that had migrated or invaded to the lower chambers were fixed with methyl alcohol, stained with crystal violet, and counted under an inverted microscope (100 \times).

2.12. Mitochondrial mass analysis

Transmission electronic microscopy (TEM) was performed at Service Biotechnology Co., Ltd. (China). Briefly, cells were fixed in 2.5% glutaraldehyde and postfixed in 1% osmium tetroxide/phosphate buffer (pH 7.4). Then, the cells were dehydrated in graded ethanol and embedded. Sections (60–80 nm) were sliced and stained with a 2% uranium acetate-saturated alcohol solution and 2.6% lead citrate solution. The cells were observed under a transmission electron microscope (HT7800, HITACHI).

Mito-Tracker Red (Invitrogen) was used to measure the mitochondrial mass. Cells stably overexpressing the vector or CES2 were seeded in 6-well plates and incubated with Mito-Tracker Red for 30 min and Hoechst 33342 (Invitrogen) for 5–10 min. The fluorescence signals were recorded using laser confocal microscope (Olympus FV3000).

2.13. Flow cytometry analysis

For ROS detection, an ROS Assay Kit (Beyotime) was used according to the manufacturer's instructions. Cells stably overexpressing the vector or CES2 were harvested and incubated with 2',7'-dichlorofluorescein diacetate (DCFH-DA, 20 μ M) or Rosup (50 mg/ml) for 20 min. Rosup was used as a positive control for ROS detection. Then, cells were washed with PBS, and the fluorescence signals were recorded using flow cytometry (Cytoflex, Beckman Coulter).

For the apoptosis assay, cells stably overexpressing the vector or CES2 were seeded in 60 mm dishes. After incubating with serum-free medium for 24 h, the cells were harvested. An Annexin V-FITC/PI Apoptosis Detection Kit (KeyGEN BioTECH) was used to detect the apoptotic cells. The flow cytometer was performed to count apoptotic cells.

The mitochondrial membrane potential (MMP) was determined using mitochondrial membrane potential assay kit with JC-1 (Beyotime). When the MMP level decreases, J-aggregates form (fluorescing red) are released from mitochondria, and they then monomers (fluorescing green) in the cytoplasm. OSCC cells were collected and dyed with JC-1 for 20 min at 37 °C. Next, a flow cytometer was performed to determine the intensities of the red and green fluorescence. The MMP was calculated on the basis of the ratio of red signals to green signals.

2.14. Oxygen consumption and glycolytic capacity

The Oxygen consumption and glycolytic capacity were measured using an XF96 Extracellular Flux Analyzer (Agilent). The XF Cell Mito Stress Test Kit (Agilent) and XF Glycolysis Stress Test Kit (Agilent) were performed based on the manufacturer's instructions. Briefly, 8×10^3 CAL33 cells or UM1 cells per well were plated onto the Seahorse 96-well plates and incubated overnight. The cell medium was replaced with the assay medium (XF Base Medium supplied with 1 mM pyruvate, 2 mM glutamine, and 10 mM glucose, adjusted to pH 7.4 with 0.1 N NaOH) before testing, according to the manufacturer's protocol. For the Cell Mito Stress Test, cells were sequentially treated with oligomycin (Oligo, a Fo-ATPase inhibitor of complex V, which can significantly reduce mitochondrial respiration; 1 μ M), the uncoupler carbonyl cyanide-p-trifluoromethoxyphenylhydrazone (FCCP; 2 μ M), rotenone (Rot) and antimycin A (0.5 μ M). For Glycolysis Stress Test, cells were sequentially treated with glucose (1 μ M), oligomycin (1 μ M) and 2-DG (2 μ M). The oxygen consumption rates and the extracellular acidification rates were recorded by the XF96 Extracellular Flux Analyzer and normalized to cell protein levels.

2.15. *In vivo* xenograft tumor model

Four-week-old BALB/c female nude mice ($n = 12$) bought from the Medical Experimental Animal Center of Guangdong Province

(Guangzhou, China) were divided into two groups (Vector and CES2). A total of 5×10^6 CAL33 cells stably overexpressing the vector or CES2 were injected into the dorsal flank of mice. After 4 days of growth, the tumor sizes were measured every 2 days for 2 weeks. Then, the mice were sacrificed. The tumors were dissected and weighed. Animal experiment was approved by the Animal Care and Use Ethics Committee of our hospital. The animal-handling protocols were conducted based on the detailed principles to minimize animal suffering.

2.16. Lipidomic and bioinformatics analysis

The lipidomic profiling was performed using an Ultra-Performance Liquid Chromatography Mass Spectrometry system (UPLC, ExionLC AD; MS, Applied Biosystems SCIEX 6500+QTRAP; Wuhan Metware Biotechnology Co., Ltd, China). Briefly, cells were harvested and lipids were extracted using a methyl tertbutyl ether and methanol mixture. The supernatants were loaded into the LC-MS/MS system. Analyst 1.6.3 software (AB Sciex) was applied to analysis the mass spectrometric data. Built-in Metware database (MWDB) and the public database of metabolite information were performed for the qualitative analysis. The lipid metabolite structural analysis was mainly based on the MassBank, KNAPSACK, HMDB, LIPID MAPS and METLIN databases. The first screening was focused on the significant features, with a p value < 0.05 , and fold change > 1.2 . The web-based tools BioPAN in LIPID MAPS (<https://lipidmaps.org/bioipan/>) and MetaboAnalyst 5.0 were applied for the enrichment analysis. Fatty acid and phosphatidylinositol concentrations were detected using a Nones-terified Free fatty acids assay kit (A042-2-1, Nanjing Jiancheng Bioengineering institute) and Human Phosphatidylinositol (PI) ELISA Kit (TL-E1418H, Telenbiotech), respectively, according to the manufacturer's instructions.

2.17. Statistical analysis

Statistical Package for the Social Sciences 19.0 software (SPSS 19.0) and R (version 4.0.3) were used for statistical analysis. Student's t -test, or chi-square and Fisher's exact tests were performed to study the continuous variables and categorical variables. The receiver operating characteristic (ROC) curve was applied to select the cut-off value for high and low CES2 expression. The Kaplan-Meier method, univariate and multivariate Cox regression analyses were used to estimate the relationship between CES2 expression levels and patient survival. The χ^2 or Fisher exact tests were used for categorical variables. Pearson's coefficient test was performed to test the relationship between the mRNA levels and methylation levels of CES2. Data presented as the mean \pm s.d. were based on results from at least three independent experiments. A P value < 0.05 was considered to be statistically significant.

3. RESULTS

3.1. Lipase CES2 downregulation is associated with poor clinical outcomes in OSCC patients

In total, 533 genes participated in FA metabolism collected in this study were downloaded from MSigDB, including genes involved in FA transport, biosynthesis, oxidation cycling, and lipolysis [15,16] (Table S2). To determine the essential FA genes involved in OSCC recurrence and metastasis, we compared the differentially expressed genes (DEGs) between OSCC and normal tissues, and patients with (RM-OSCC) and without (non-RM-OSCC) recurrence or metastasis. In contrast to the normal and non-RM-OSCC tissues, 56 genes were downregulated and 35 genes were upregulated in OSCC and were also altered in RM-OSCC tissues. In total, 257 FA genes were

downregulated and 35 were upregulated in OSCC tissues compared to the normal tissues (Table S3). In contrast to the non-RM-OSCC patients, 4 FA genes were downregulated and 2 FA genes were upregulated in RM-OSCC patients (Table S4). Notably, only one FA gene, CES2, which participates in neutral lipid hydrolysis (also called lipolysis) [7], was differentially expressed in both OSCC and RM-OSCC tissues (Figure 1A–C).

Next, the downregulation of CES2 in normal oral epithelial tissues and OSCC tissues was validated with the GSE30784, GSE31056, GSE37991, and GSE25099 cohorts (Figure 1D). The low expression of CES2 in RM-OSCC patients in the GSE67614 cohort was confirmed (Figure 1E). We further examined CES2 expression levels in OSCC cell lines and clinical specimens using qPCR, western blot and IHC assays. Both the mRNA and protein levels of CES2 were lower in OSCC cells (CAL27, CAL33, UM1, HSC3 and HSC6) than in oral keratinocyte HOKs (Figure 1F). The CES2 protein levels were also verified to be downregulated in OSCC specimens collected at our hospital (Figure 1G). Moreover, Kaplan-Meier survival analysis showed that CES2^{high} patients had better overall survival (OS) than CES2^{low} patients in the TCGA-OSCC and GSE41613 cohorts (Figure 1H). Together, we demonstrated that the downregulation of CES2 in OSCC exhibited unfavorable clinical outcomes and might play critical roles in OSCC progression.

3.2. CES2 downregulation is partially due to its promoter hypermethylation in OSCC

We searched the UCSC Genome Browser to analyze the characteristics of the CES2 genome, and found that two CpG islands (CGI 85, chr16: 66,934,127–66,935,021; CGI 32, chr16: 66,935,597–66,935,975) were located in the CES2 genome. Both CGIs showed strong H3K4me1, H3K4me3 and H3K27Ac enrichment (the histone modification present at promoters), and the DNase I hypersensitivity signal and the regulatory elements (enhancers and promoters) signals in seven cell lines in ENCODE according to GeneHancer, implying that the CGIs in CES2 might function as alternative promoters [14] (Figure 2A). Based on the Human Methylation 450K BeadChip (Illumina) data for the TCGA-OSCC, 22 methylation probes are located in the CES2 genomic sequence. A proportion of 68% probes are located in CpG islands (CGIs) and 81% probes are located in promoter regions (TSS200 and TSS1500) (Figure 2B, Table S5). We analyzed the relationship between the methylation level of CES2 promoter and its mRNA level in OSCC using cBioportal online tool, and identified a weak inverse correlation between them (Figure 2C). In comparison with the methylation levels in the normal tissues, the hypermethylation at cg26785230 (TSS1500, promoter) and cg09203199 (body) and the hypomethylation at cg03647619 (3'UTR) in OSCC tissues were identified in TCGA, GSE75537 and GSE87053 cohorts (Figure 2D). The methylation levels at cg26785230 in the CGI 32 were weakly and inversely correlated with CES2 mRNA levels (Figure 2E). Importantly, treating OSCC cells with a demethylation agent (5-Aza, 2.5 μM) partially restored CES2 mRNA levels in OSCC cell lines (Figure 2F). Therefore, these findings demonstrated that promoter hypermethylation might partially contribute to CES2 downregulation in OSCC.

3.3. CES2 restrains cell viability, migration and invasion *in vitro* and tumor growth *in vivo* in OSCC

To identify the molecular functions of CES2 in OSCC cells, we stably overexpressed CES2 expression in CAL33 and UM1 cells (Figure 3A–B), and transiently silenced its expression in HSC3 and CAL27 cells (Figure 3C–D). CCK-8 assays showed that the OSCC cells with CES2 overexpression showed lower cell viability, while cells with CES2

silenced showed higher cell viability than those in the negative control groups (Figure 3E–F). Transwell assays without or with Matrigel implied that restoring CES2 expression obviously suppressed OSCC cell migration and invasion, and that knocking down CES2 expression exerted the opposite effects (Figure 3G–J).

CAL33 cells stably overexpressing CES2 or the empty vector were injected into the dorsal flank of BALB/c nude mice to investigate the effects of CES2 on OSCC cell tumor growth *in vivo*. The volumes, growth rates and weights of the tumors were calculated. Compared to the tumors in the vector group, the tumors in the CES2 overexpression group were smaller, grew slower and weighed less (Figure 3K–M). In summary, CES2 acted as a tumor suppressor gene in OSCC progression.

3.4. CES2 suppresses OSCC malignancy progression by hydrolyzing neutral DGs, reducing membrane structure PLs and releasing toxic lipids

To identify the lipase activity of CES2 in OSCC cells, MS and orthogonal partial least squares-discriminant analysis (OPLS-DA) were performed to determine the lipidomic differences between CES2 overexpression and vector overexpression CAL33 cells. Altogether, 540 lipids with different lengths and saturation concentrations were identified, with 62 downregulated and 109 upregulated in CES2 overexpression cells (Figures 4A, S1A–B and Table S6). Unexpectedly, the neutral lipid TGs were found to be obviously accumulated in CES2 overexpression OSCC cells, in contrast to findings in the obesity and NAFLD (Figures 4A–C and S1B). Besides, few intermediate substrate MGs were found in our lipidomic profile of OSCC cells (Figures 4A–C and S1A). The remarkably downregulated neutral lipids were DGs, along with the increase of free FAs in CES2 overexpression cells (Figures 4A–E and S1B). The levels of acyl-carnitines (CARs), which are converted from free FAs by carnitine palmitoyltransferases and shuttled into mitochondria for oxidation (a process called fatty acid oxidation, FAO) [17,18], were also obviously elevated (Figures 4A–C and S1B). Given that free FAs constitute the backbone structure of complex lipids and are the main active toxic lipid class, the increase in FA pool contents were validated by an additional FA detection kit in CES2 overexpression cells (Figure 4F). Thus, these data suggested that CES2 might hydrolyze DGs to release free FAs and then convert these FAs into CARs for FAO in OSCC cells.

Phospholipids (PLs), cholesterol (CEs) and sphingolipids are the major constituents of biological membranes [19]. PLs include phosphatidylcholines (PCs), phosphatidylethanolamines (PEs), phosphatidylserines (PSs), phosphatidylinositols (PIs) and phosphatidic acids (PAs). Sphingomyelins (SMs) are synthesized from ceramide (CER) and the phosphocholine head group of PCs. In CES2 overexpressing cells, our lipidomic data showed that the levels of membrane PLs and their substrates, including PCs, PEs, PGs, PSs, lysophosphatidylcholines (LPCs), lysophosphatidylethanolamines (LPEs) and PAs, were remarkably reduced, while SMs, CERs and CEs accumulated (Figures 4A–C and S1B–E). In addition, the PC/SM ratio was reduced in CES2 overexpression cells, implying decreased cell membrane fluidity (Figure 4G).

Lipids can be substrates, products or intermediates and are interconnected through complex metabolic pathways. DGs can directly interact with CDP-choline or CDP-ethanolamine to form PCs or PEs. Phosphorylation of the free hydroxyl group of DGs produces PAs to form other PLs. In turn, PLs are substrates for the generation of DGs [20,21]. Sphingomyelins (SMs) are synthesized using ceramides (CERs) and the phosphocholine head group from PCs. In the SM formation reaction, DGs are also produced. Cholesterol and

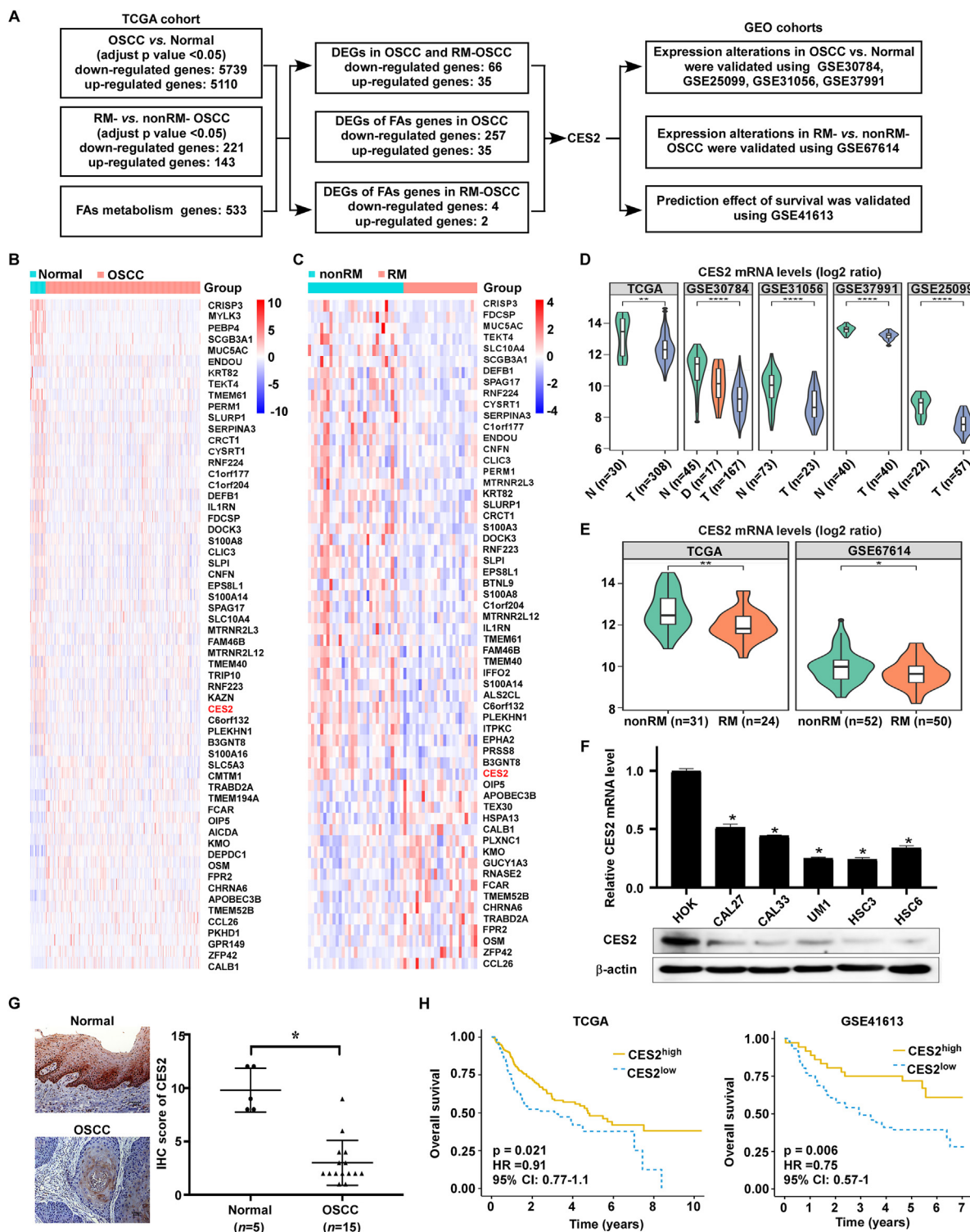


Figure 1: Lipase CES2 downregulation is associated with poor clinical outcomes in OSCC patients. (A) The analytic pipeline for identifying the alteration of FA metabolism genes in advanced OSCC. (B, C) Heatmaps showing altered expression of differentially expressed genes both in OSCC (B) and RM-OSCC (C). Red words: FA genes. (D) The mRNA levels of CES2 in normal (N), dysplasia (D) and OSCC (T) tissues based on TCGA, GSE30784, GSE31056, GSE37991 and GSE25099 datasets. (E) The mRNA levels of CES2 in OSCC with (RM-) or without (non-RM) recurrence or metastasis based on the TCGA and GSE67614 datasets. (F) Relative mRNA and protein levels of CES2 in human oral HOKs and OSCC cells (CAL27, CAL33, UM1, HSC3 and HSC6 cells) were measured by qPCR and western blot assays, respectively. β -Actin was used as an endogenous control. (G) Immunohistochemical staining ($\times 200$) and statistical analysis of CES2 levels in normal and OSCC tissues. (H) Kaplan–Meier analysis was performed to determine overall survival according to the mRNA levels of CES (low versus high) in OSCC patients in the TCGA cohort ($n = 343$) and GSE41613 ($n = 97$) cohort. *, $P < 0.05$; Student's t tests. HRs and P values were calculated by univariate Cox regression analysis.

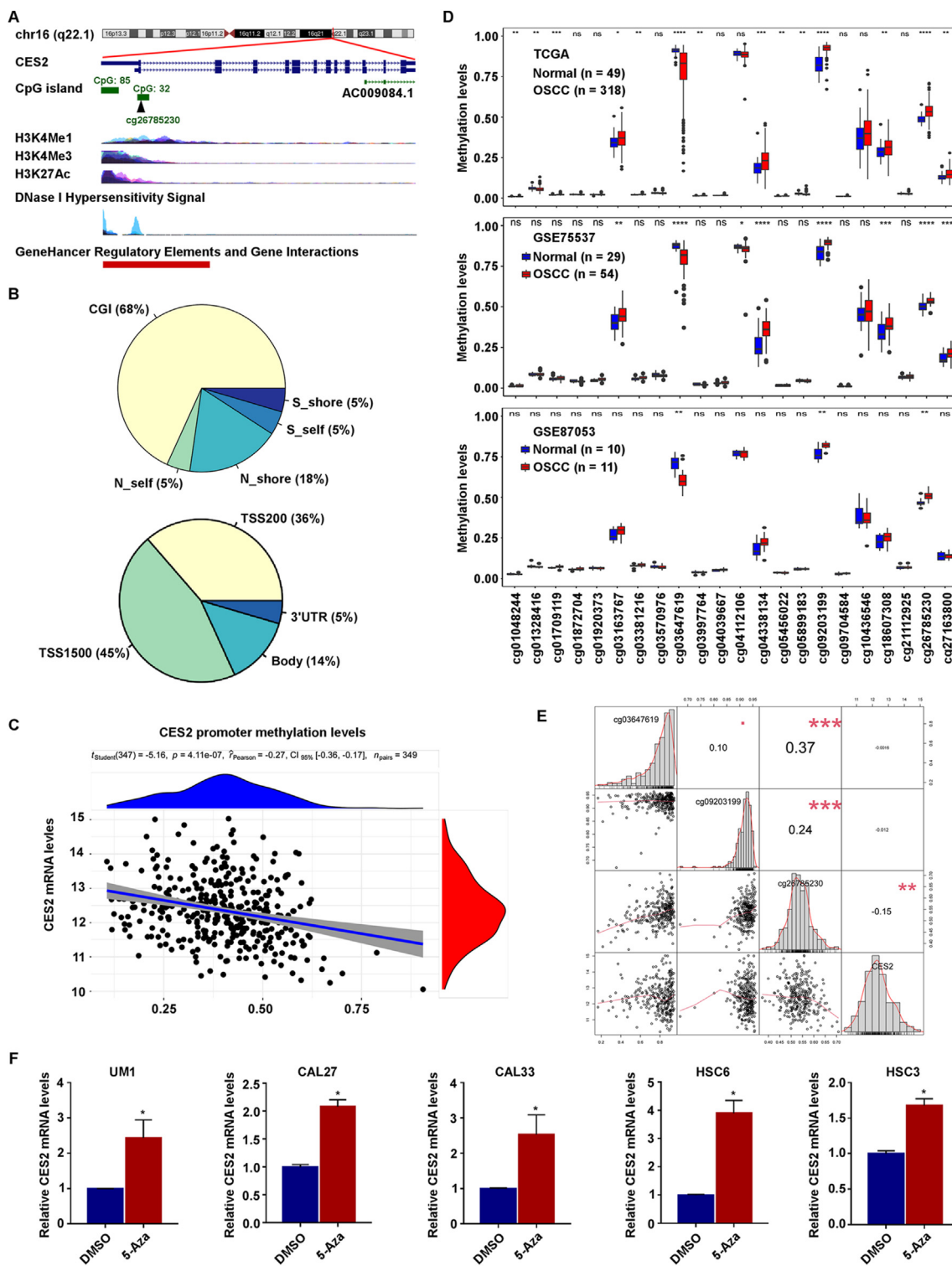


Figure 2: CES2 downregulation is associated with promoter hypermethylation in OSCC. The genomic features of CES2 as indicated in the UCSC genome browser. (B) The genomic distribution of CG probes in the Human Methylation 450K BeadChip (Illumina). (C) The relationship between the methylation levels of the CES2 promoter and its mRNA levels in OSCC was analyzed with the cBioPortal online tool. (D) The methylation levels of CES2 CG probes were identified in normal and OSCC tissues of the TCGA, GSE75537 and GSE87053 cohorts. (E) The relationship between the methylation levels of the CES2 CG probes (cg03647619, cg09203199 and cg26785230) and their mRNA levels in OSCC was analyzed by Pearson correlation analysis ($n = 349$). The rightmost column shows the correlation coefficient (r); **, $P < 0.01$. (F) Relative mRNA levels of CES2 in OSCC cell lines treated with DMSO or 5-aza (2.5 μ m). The mean \pm s.d.; *, $P < 0.05$; Student's t tests.

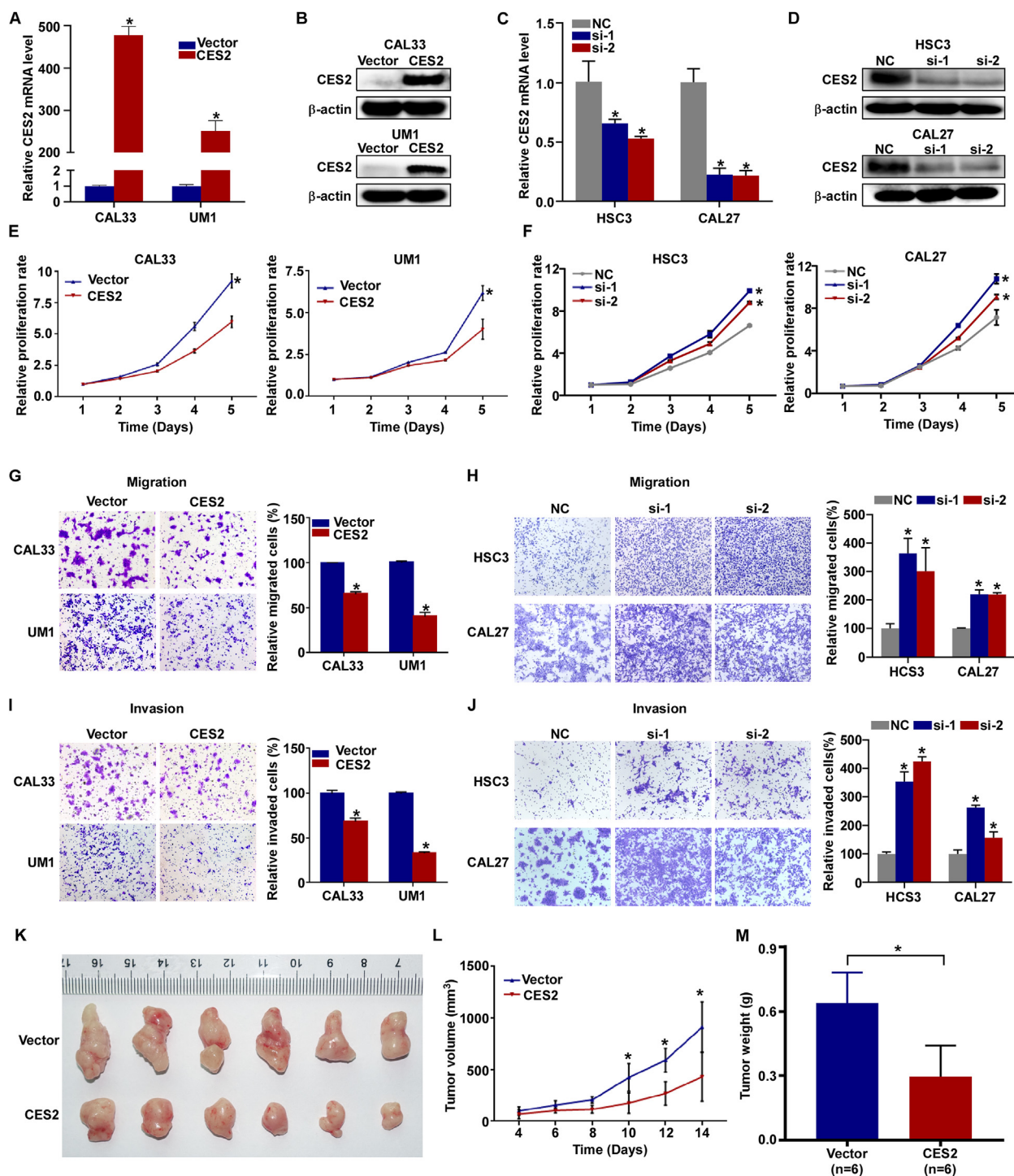


Figure 3: CES2 represses OSCC cell progression *in vitro* and *in vivo*. CAL33 and UM1 cells stably overexpressing the empty vector or CES2 and HSC3 and CAL27 cells with the negative control (NC) or transiently silenced CES2 (si-1 and si-2) were used to study the biological function of CES2. (A–D) The transfection efficiencies of the vector and CES2 plasmids and siRNA effects (NC, si-1 and si-2) were examined by qPCR and western blot assays, respectively. The relative mRNA (A, C) and protein (B, D) levels of CES2. β-Actin was used as the endogenous control. (E, F) The relative proliferation rates of stable empty vector- or CES2-overexpressed cells were measured by CCK-8 assays (E), and the relative proliferation rates of these cells were measured in cells with the NC or transiently silenced CES2 (si-1 and si-2) (F). (G–J) Migratory and invasive abilities were detected with Transwell assays without (G, H) and with Matrigel (I, J), respectively, in stably empty vector- or CES2- overexpressing cells and in cells with the NC or CES2 transiently silenced (si-1 and si-2). (K–M) Representative images of tumor nodules (K), quantification of tumor volumes (L) and weights (M) in mouse xenografts. The mean \pm s.d.; *, $P < 0.05$; Student's t tests.

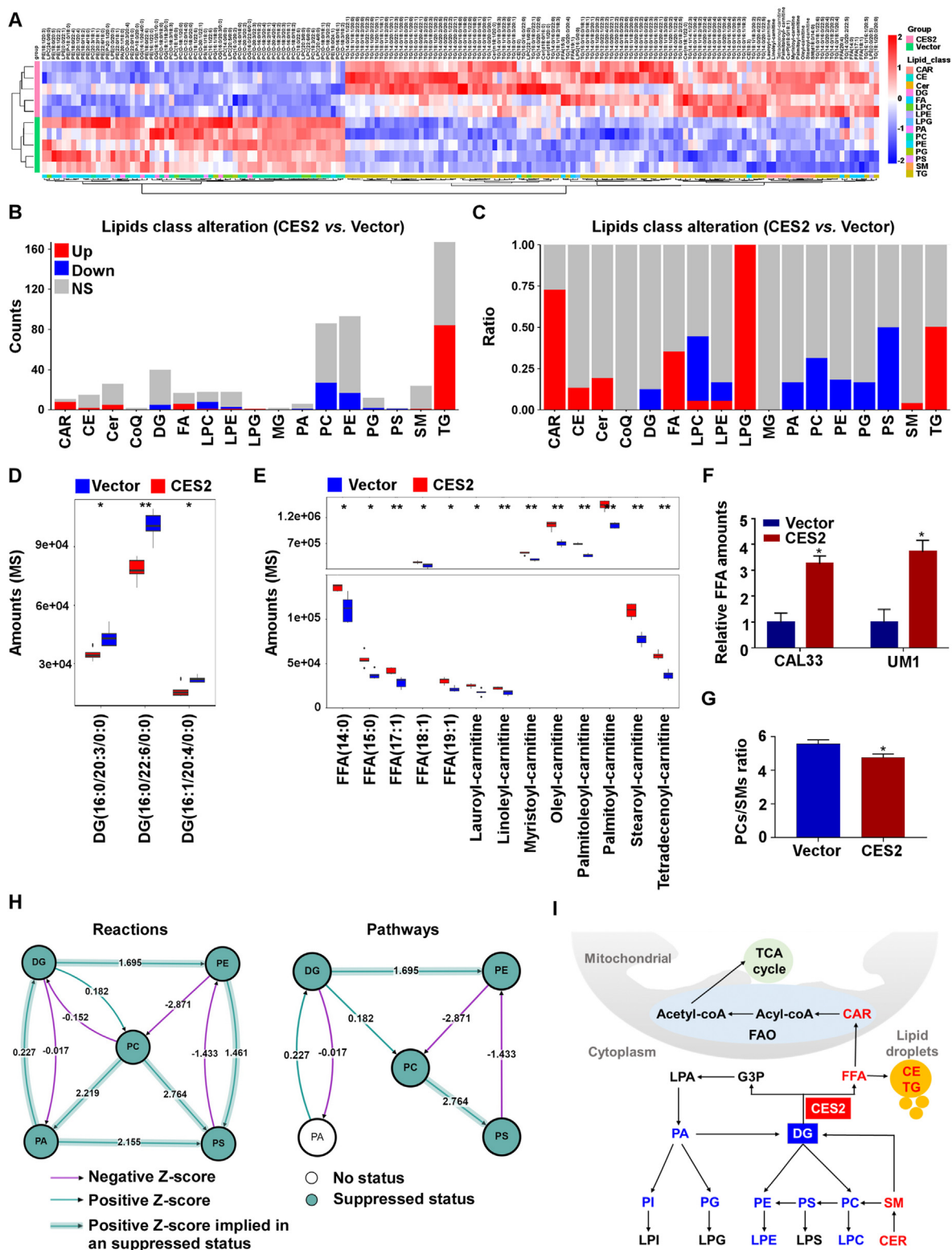


Figure 4: CES2 reprograms lipid homeostasis in OSCC. Mass spectrometry was performed to analyze the lipidome in CAL33 cells overexpressing CES2 or the empty vector. (A) Heatmap showing differences in the contents of lipids in CAL33 cells with CES2 and empty vector overexpression. (B, C) The numbers (B) and proportions (C) of lipids identified and altered in CES2-overexpressing cells in contrast to those in empty vector-expressing cells. (D, E) Levels of representative individual DGs (D), FAs and CARs (E) in CES2- and empty vector-overexpressing cells. (F) The representative levels of FFAs in CAL33 and UM1 cells with CES2 or empty vector overexpression. (G) The ratio of PCs/SMS in CAL33 cells with CES2 or empty vector overexpression. (H) The reactions and pathways related to different lipid contents in CAL33 cells with CES2 and empty vector overexpression. (I) Summary of the lipid profile changes in CAL33 cells with CES2 and empty vector overexpression. The mean \pm s.d.; *, $P < 0.05$; Student's *t* tests.

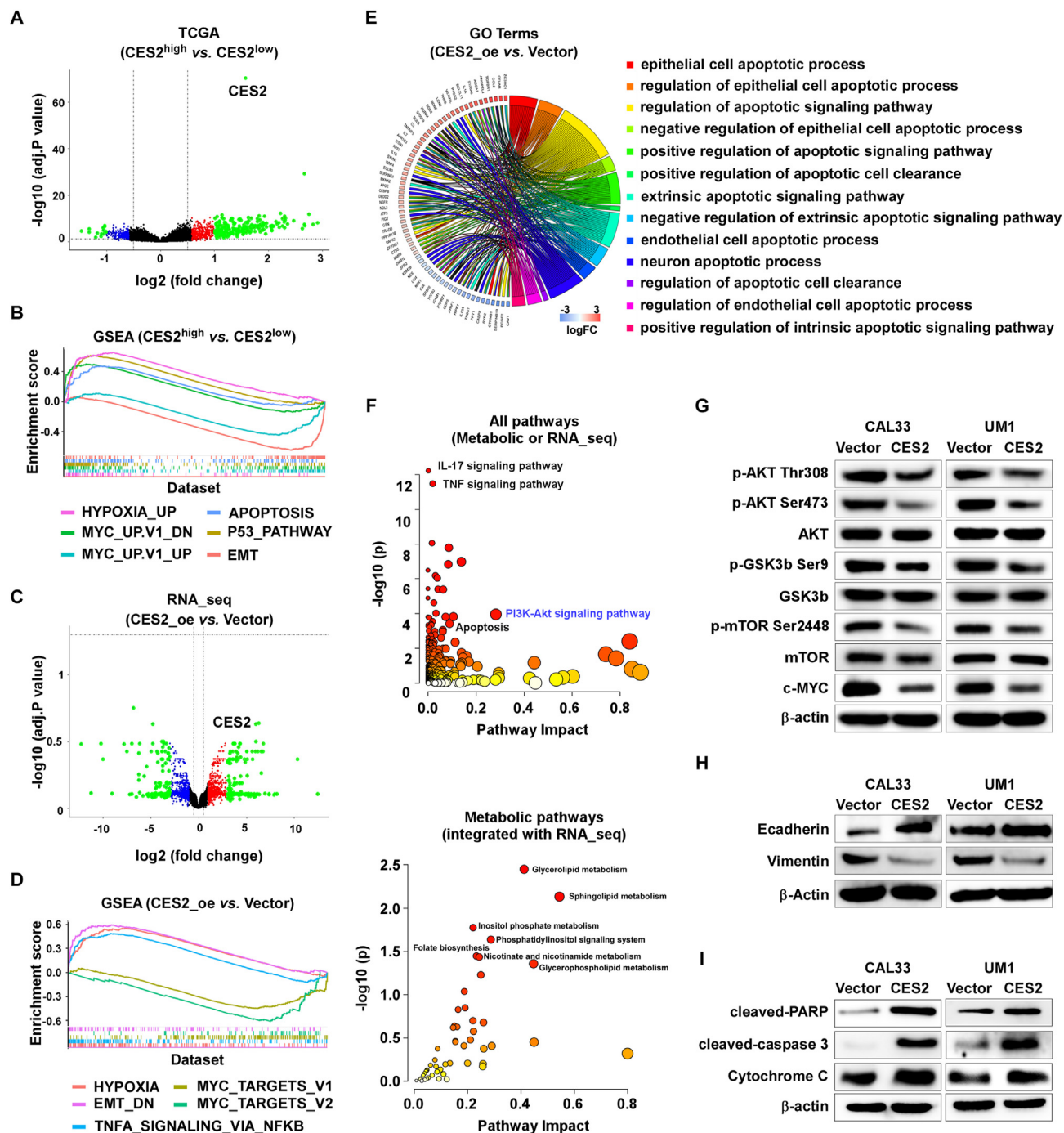


Figure 5: CES2 represses the PI3K/AKT/MYC signaling pathway and induces apoptotic signaling in OSCC. (A, B) A volcano plot (A) and GSEA (B) showing the transcriptome differences between patients with CES2^{high} (n = 110) and CES2^{low} (n = 239) in the TCGA cohort. (C–E) RNA-seq profiling was performed with stably empty vector- and CES2-overexpressing cells. The volcano plot (C), GSEA (D) and GO analysis (E) showing the transcriptome differences between stably empty vector- and CES2-overexpressing cells. (F) Pathways of the differentially expressed genes and/or lipids between CES2- and empty vector-overexpressing cells as identified by MetaboAnalyst 5.0 based on lipidomic and RNA-seq data. (G) Representative levels of PIs as determined by ELISAs with CAL33 and UM1 cells in which CES2 or the empty vector was overexpressed. (H–J) The protein levels of the PI3K/AKT/MYC signaling pathway, including p-AKT (Thr308 and Ser473), p-mTOR (Ser2448), p-GSK3 β (Ser9) and MYC (H); EMT markers, including E-cadherin and Vimentin (I); and endogenous apoptosis markers, including cleaved PARP, cleaved caspase 3 and cytochrome C (J), were measured by western blotting. β -Actin was used as the loading control. The mean \pm s.d.; *, $P < 0.05$; Student's t tests.

sphingolipids often act as functional pairs due to their interactions. To better explore the lipidome metabolic pathways altered by CES2, we applied BioPAN, a web-based tool in LIPID MAPS (<https://lipidmaps.org/biopan/>) [22]. In CES2 overexpressing cells, the DG \rightarrow PE \rightarrow PS

reactions were identified to be one of the most suppressed reactions, while PE \rightarrow PC \rightarrow DG \rightarrow PA reactions were the most active reaction (Figure 4H, Table S7). Furthermore, the DG \rightarrow PE pathway was one of the most suppressed pathways by CES2 (Figure 4H, Table S8),

implying that the degradation of membrane PLs was accelerated, while PL synthesis was diminished in CES2 overexpressing cells. Collectively, we demonstrated that CES2 lipase reprogrammed lipid metabolism in OSCC cells by hydrolyzing the neutral lipid DGs to release free FAs for consumption in FAO: on the one hand, DGs decomposition weakened membrane PL synthesis and decreased a diverse range of signaling lipids contents (e.g., DGs, PLs and their substrates); on the other hand, the levels of several bioactive lipids (e.g., FAs, CARs and CERs) were increased in OSCC cells (Figure 4).

3.5. CES2 induces apoptotic signals and represses the PI3K/AKT/MYC oncogenic signaling pathway by reprogramming lipid metabolism

We wondered whether CES2-mediated lipid metabolism remodeling affect the biological functions of OSCC cells. First, we compared transcriptome differences between CES2^{high} and CES2^{low} OSCC patients in the TCGA cohort. A total of 824 differentially expressed genes were identified between the two groups (Figures 5A, S2 and Table S8). GSEA analysis indicated that apoptosis, hypoxia_up, P53_pathway, and MYC_UP.V1_DN were activated, while MYC_UP.V1_UP and EMT were suppressed in CES2^{high} patients (Figure 5B).

Second, we compared the transcriptome differences between OSCC cells with CES2 overexpression and those with vector overexpression. In contrast to the vector group, 911 genes were differentially expressed, with 491 genes upregulated and 420 genes down-regulated, in the CES2 overexpression group (Figures 5C, S3A, and Table S9). Similarly, GSEA enrichment analysis revealed that hypoxia-related genes were activated, while MYC_targets_V1 and _V2 and EMT_DN were suppressed in CES2 overexpressing cells (Figure 5D). GO and KEGG analysis showed that the differentially expressed genes were involved in activating a series of apoptotic processes (Figures 5E and S3B).

Third, the Joint Pathway Analysis module of MetaboAnalyst 5.0, which is based on lipidomic and RNA-seq data, was used to explore the pathways of differentially expressed genes and differentially abundant lipids between vector and CES2 overexpressing cells [23]. The combined analysis showed that transcriptome and lipidomic differences were obvious in glycerophospholipid metabolism, glycerolipid metabolism, sphingolipid metabolism, and phosphatidylinositol signaling systems (Figure 5F and Table S10). The PI3K/AKT and apoptosis-associated pathways were found to be enriched with the genes differentially expressed between CES2- and vector-overexpressing cells (Figure 5F and Table S11). Considering that PIs play critical roles in activating PI3K/AKT signaling, we additionally examined the total PI content, and the results showed that CES2-overexpression cells exhibited lower levels of total PIs than vector cells (Figure S4).

After the GSEA and Joint Pathway analysis, western blotting was applied to validate the effects of CES2 on the PI3K/AKT and MYC signaling pathways, the EMT and apoptotic biomarkers. We confirmed that restoring CES2 expression reduced the protein levels of p-AKT (Thr308 and Ser473), p-GSK3 β (Ser9), p-mTOR (Ser2448) and MYC, while silencing CES2 led to the opposite effects, implying that CES2 expression decreased the levels of signaling lipids to repress the activation of PI3K/AKT and downstream MYC signaling pathways, the most commonly activated oncogenic pathways in OSCC progression [1,15] (Figures 5G and S5). The level of the epithelial marker E-cadherin was upregulated and that of the mesenchymal marker Vimentin was decreased in CES2 overexpressing cells, demonstrating that CES2 inhibited cell migration and invasion partially by suppressing the EMT in OSCC cells (Figure 5H). More importantly, the levels of the endogenous apoptosis biomarkers, cleaved-PARP, cleaved-caspase 3 and

cytochrome C, were increased by CES2, which might be results of increased toxic lipid-induced lipotoxicity (Figure 5I). Collectively, these data illustrated that CES2 repressed the PI3K/AKT/MYC oncogenic signaling pathway and induced apoptotic signaling by reprogramming lipid metabolism.

3.6. CES2 disrupts lipid homeostasis and induces severe oxidative stress leading to mitochondrial dysfunction and apoptosis in OSCC

The aforementioned lipidomic profile indicated that CES2 accumulated FAs and CARs, which were consumed in FAO and might increase the oxidative stress in mitochondria. Considering the central role played by mitochondria in maintaining FA homeostasis, particularly in resisting lipotoxicity and inducing apoptosis, we examined the influences of CES2 on mitochondria. TEM and MitoTracker Red staining micrographs showed that the structure of mitochondria was profound changed by CES2 overexpression. In contrast to the tubular mitochondria observed in the empty vector group, CES2-overexpression cells showed fragmented and lost cristae in mitochondria, reduced mitochondrial mass, and reduced mitochondrial DNA (mtDNA) levels (Figure 6A–C). The mitochondrial membrane potential was also attenuated, while the ROS and apoptotic cells were increased in CES2 overexpressing cells (Figure 6D–F). Using a Seahorse extracellular flux analyzer, we observed that cells with CES2 overexpression had a lower oxygen consumption rate (OCR) both in the basal and maximal-uncoupled states, and lower mitochondrial ATP production than cells with vector overexpression (Figure 6G). Little difference was seen in the extracellular acidification rate (ECAR) during glycolysis between the CES2 overexpression group and the vector group, indicating that no compensatory mechanism for energy deficiency had been activated (Figure S6). Additionally, silencing CES2 increased the mtDNA contents and mitochondrial membrane potential, and reduced the number of apoptotic cells (Figure 6I–K). Together, these findings demonstrated that CES2 increased toxic lipid generation to induce oxidative stress and mitochondrial dysfunction, which ultimately induced cell apoptosis in OSCC.

3.7. CES2 suppresses OSCC progression via MYC-mediated oncogenic signaling inactivation

Given that the MYC-associated transcription network has been commonly recognized to play a central role in lipid and mitochondrial metabolism regulation [24], we wondered whether restoring MYC expression can abrogate the tumor-suppressing effect of CES2 in OSCC cells. Therefore, MYC expression was restored in CES2 overexpressing cells (Figure 7A). CCK-8 and Transwell assays showed that cell viability and migratory and invasive abilities originally suppressed by CES2 were rescued by restored MYC expression (Figure 7B–D). Furthermore, MYC restored the mitochondrial morphology that had been disrupted by CES2 (Figure 7E). Moreover, MYC decreased the number of apoptotic cells induced by CES2 overexpression (Figure 7F). Hence, these findings demonstrated that MYC is a functional target of CES2 in OSCC cells.

4. DISCUSSION

Lipid metabolism reprogramming is well known to play essential roles in OSCC progression, which is precisely regulated by FAs in the intracellular FA pool. However, how OSCC cells regulate lipid homeostasis to prevent nonesterified FA-induced lipotoxicity has rarely been investigated. The present study comprehensively analyzed the transcriptome alterations of genes that participate in keeping FA pool homeostasis in OSCC with recurrence or metastasis and demonstrated

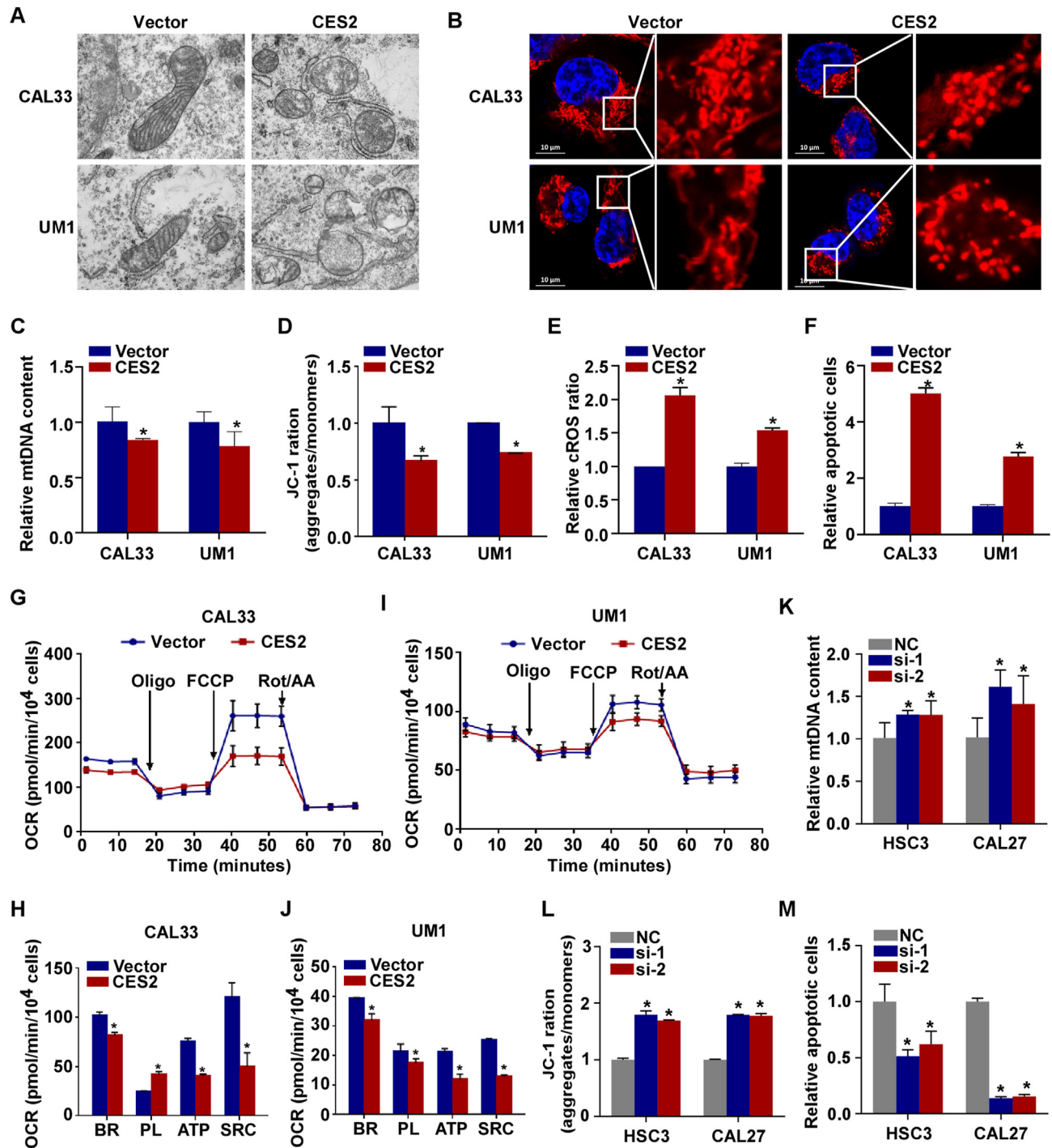


Figure 6: CES2 induces oxidative stress, mitochondrial dysfunction and apoptosis in OSCC. (A–B) The mitochondrial morphology was affected by CES2 as shown via TEM (A) and by stained with MitoTracker Red, as visualized via a laser confocal microscopy (B). (C) The mtDNA contents in CAL33 and UM1 cells with empty vector or CES2 overexpression were examined by qPCR. (D–F) The mitochondrial membrane potential (D), ROS levels (E) and number of apoptotic CAL33 and UM1 cells with empty vector or CES2 overexpression (F) were determined by flow cytometry. (G–J) The oxygen consumption rate (OCR) in basal and maximal-uncoupled states and mitochondrial ATP production in CAL33 and UM1 cells with CES2 or empty vector overexpression were determined with a Seahorse XF analyzer. (K–M) The mtDNA contents (K), mitochondrial membrane potential (L) and number of apoptotic cells (M) HSC3 and CAL27 cells with NC or CES2 silencing (si-1 and si-2). The mean \pm s.d.; *, $P < 0.05$; Student's *t* tests.

that the downregulation of CES2 expression was the key event. OSCC patients with low CES2 mRNA levels exhibited poor clinical outcomes. CES2 hydrolyzed DGs and released toxic FAs for consumption during mitochondrial oxidation and promoted ROS production; number of DGs

were thus reduced, which in turn repressed membrane PL synthesis to further aggravate mitochondrial dysfunction and release apoptotic molecules that induce OSCC cell death. Moreover, the reduction in the number of signaling lipids suppressed the PI3K/AKT/MYC signaling

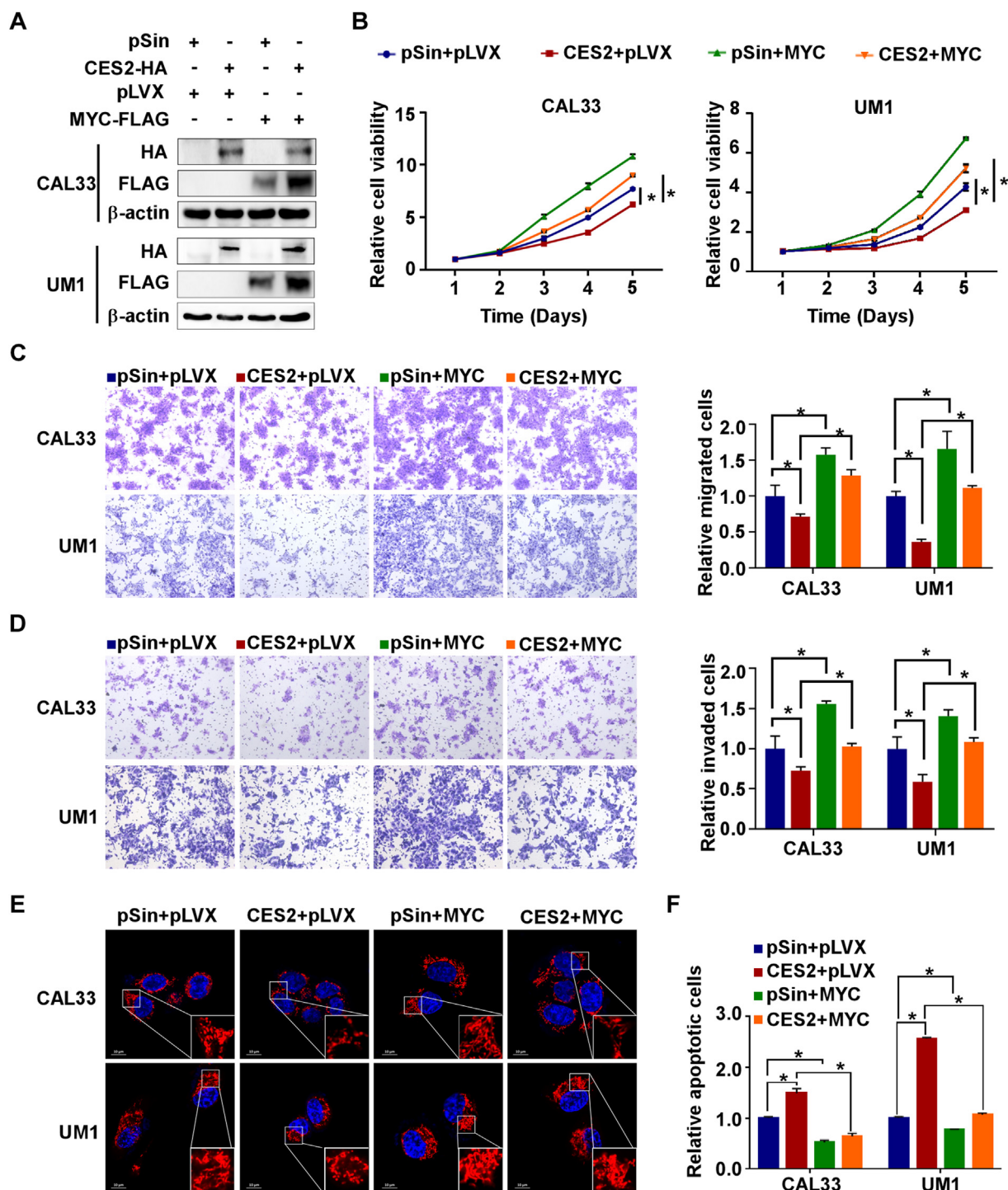


Figure 7: CES2 suppresses tumor progression by repressing MYC activity. CAL33 and UM1 cells stably overexpressing CES2-HA or empty control plasmid (pSin) were transfected with MYC-FLAG or empty control plasmid (pLVX). (A) The protein levels of HA and FLAG were confirmed by western blotting. β -Actin was used as the loading control. (B) Cell viability was measured by CCK-8 assay. (C, D) The migratory (C) and invasive (D) abilities were detected using Transwell assays without or with Matrigel, respectively. (E) The mitochondria were stained with MitoTracker Red and the morphology was observed via a laser confocal microscopy. (F) The number of apoptotic cells were determined by flow cytometry. The mean \pm s.d.; *, $P < 0.05$; Student's t tests.

pathway, which ultimately reduced mitochondrial mass and repressed tumor progression (Figure 8).

Despite their roles in essential cellular functions, FAs at high concentrations are toxic due to their limited solubility and amphipathic

nature, adverse impact on cellular acid-base homeostasis, and generation of highly bioactive, cytotoxic lipid species [25,26]. These deleterious effects, in turn, damage biological membranes, induce mitochondrial dysfunction, and increase oxidative stress and the cell

death rate. As a countermeasure, to ensure sufficient FA flux for rapid growth and prevent redundant and toxic FA accumulation, cancer cells evolve an efficient buffer system to balance intracellular FA generation and consumption. Cancer cells acquire FAs from a range of extra- and intracellular sources [15]. The extracellular pathways include protein-mediated uptake and micropinocytosis. The intracellular pathways include de novo synthesis from carbohydrate and protein metabolites and lipolysis of intracellular lipids. The consumption patterns include channeling FAs into mitochondria for use in oxidation and esterification with glycerol to generate inert neutral lipids. In contrast to lipogenesis, which has drawn much attention, the roles played by lipolysis in maintaining FA and complex lipid homeostasis in tumor progression are only now coming to light. In the present study, we identified that the lipase CES2 played critical roles in maintaining FA pool homeostasis in OSCC.

The expression levels of CES2 are heterogeneous in human cancers. Downregulation of CES2 expression has been found in cholangiocarcinoma [27], while CES2 upregulation has been found in pancreatic ductal adenocarcinoma (PDAC) [28,29] and neuroblastoma [30]. Over decades, CES2 has been found to be correlated with cancer patient clinical outcomes because it plays a role in activating the metabolism of anticancer drugs. For example, CES2 activated the metabolism of the prodrug CPT-11, inducing the induction of the active form SN-38, which exerts an antitumor effect on colon cancer [31]. In patients with high CES2 mRNA expression, neuroblastoma cells were related to advanced disease and were more sensitive to CPT-11 [30]. However, the mechanisms regulating the altered expression and biological role played by CES2 in OSCC are still unknown. In this study, we found that the lipase CES2 was obviously downregulated in OSCC patients, especially those with cancer recurrence or metastasis. CES2^{low} patients exhibited poor OS. Restoring CES2 expression led to reduced cell proliferation, migration, and invasion and induced apoptosis in OSCC. Furthermore, mitochondria were fragmented, mtDNA content and the membrane potential were all reduced, and ROS accumulated in CES2 overexpressing OSCC cells. Thus, we demonstrated that the lipase CES2 suppressed OSCC progression by inducing mitochondrial dysfunction.

In mouse models of NAFLD and obesity, CES2 has been reported to maintain hepatic TG homeostasis by hydrolyzing TG, which induced fatty acid oxidation (FAO) enhancement, lipogenesis repression, endoplasmic reticulum (ER) stress reduction and increased glucose

tolerance [8,9]. However, Gabriel Chalhoub et al. emphasized that CES2 induced more efficient hydrolysis of DGs and MGs than TGs [32]. In our study, few intermediate MGs were identified in OSCC cells. Overexpression of CES2 significantly reduced the number of DGs and increased that of TGs, implying that CES2 mainly hydrolyzed DGs in OSCC cells. Generally, DGs are metabolized in three ways, namely, hydrolysis by diacylglycerol lipase (DGLs) to generate MGs and FAs, the addition of CDP-choline or-ethanolamine to generate PCs or PEs, or phosphorylation of the free hydroxyl group to produce PAs which can be converted to other PLs [33]. In OSCC cells, we found that CES2 increased the levels of FAs and decreased the levels of several PLs and substrates (e.g., PCs, PEs, PGs, PSs, Pls, LPCs, LPEs and PAs). Thus, we demonstrated that CES2 mainly induced DGs degradation to generate FAs, leading to lower PL production. On the one hand, the released FAs were converted to CARs and shuttled into mitochondria for consumption during oxidation, which led a marked increase in ROS, which damaged cellular membranes and induced mitochondrial dysfunction [18]. On the other hand, reduction in the PL levels attenuated the synthesis of membrane structure lipids required for to repair a damaged membrane. Eventually, the CES2 overexpression cells suffered catastrophic injury which damaged mitochondrial oxidative capacity, resulting in the accumulation of FAs and CARs, thereby leading to cytochrome-c release from damaged mitochondria and triggering irreversible apoptotic cell death. Notably, instead of hydrolyzing, TGs accumulated in CES2 overexpressing cells might be a result of the decreasing utilization by damaged mitochondria.

Cancer cells directly regulate lipid metabolism to upregulate many oncogenic signaling pathways and thus maintain their malignancy [34]. Membrane lipid DGs are well-established second messengers that can activate several signaling proteins, such as PKCs, PKD, Ras GRPs and certain transient receptor potential channels [33]. Although Pls constitute only approximately 1% of the lipids in the eukaryotic plasma membrane, they play major roles as signaling molecules to activate PI3K/AKT/MYC signaling pathways. PAs can bind to key cellular effectors to activate enzymes, such as mTORC1 and mTORC2, which phosphorylate several members of the AGC kinase family, e.g., AKT, to control various cellular processes [2]. Following the degradation of DGs, PLs and PAs, it was not surprising that CES2 overexpression suppressed the PI3K/AKT/MYC signaling pathway in OSCC cells. In summary, this study demonstrates that CES2 plays an essential role in maintaining lipid homeostasis to inhibit tumor progression in OSCC.

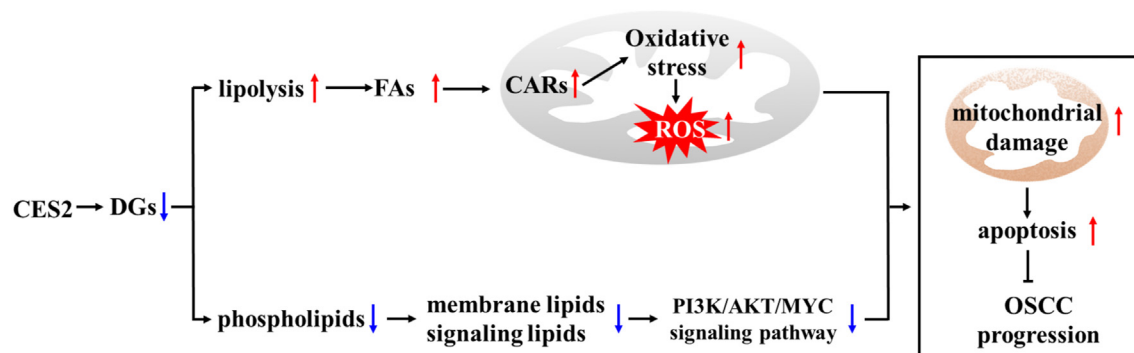


Figure 8: Schematic model showing the role played by CES2 in regulating lipid homeostasis and OSCC progression. Generally, DGs are hydrolyzed to generate FAs and are generated to produce membrane phospholipids. CES2 enhances the hydrolysis of DGs to generate excessive FAs, inducing a marked increase in ROS levels and leading to mitochondrial damage; in addition, fewer DGs were available for phospholipid synthesis, reducing the signaling lipids available to activate the oncogenic PI3K/AKT/MYC signaling pathway and generate cellular membrane structures that repair damaged membrane, which inevitably leads to apoptosis. OSCC cells with decreased CES2 expression produce moderate amounts of FAs to promote cell growth and metastasis and prevent lipotoxicity.

OSCC cells show downregulated CES2, which ensures an adequate supply of second messengers for oncogenic pathway activation and avoid lipotoxicity. Therefore, CES2 may be a potential therapeutic target for OSCC.

ETHICS COMMITTEE APPROVAL AND PATIENT CONSENT

This research was authorized by the Institutional Ethical Review Boards of Hospital of Stomatology, Sun Yat-sen University. The written informed consents were provided by all patients participated in this study. The animal experiments were approved by the Animal Care and Use Ethnic Committee of Hospital of Stomatology, Sun Yat-sen University.

CONSENT FOR PUBLICATION

Not applicable.

FUNDING

This work was supported by grants from the Natural Science Foundation of Guangdong Province (2019A1515010679); the Guangdong Basic and Applied Basic Research Foundation (2021A1515111020); the Science and Technology Projects in Guangzhou (202206080009); the Guangdong Financial Fund for High-Caliber Hospital Construction (174-2018-XMZC-0001-03-0125/C-08); China Postdoctoral Science Foundation (2019M653231, 2021M703688); the National Natural Science Foundation of China (82103555, 81700979). The funders had no role in the study design, data collection, analysis, decision to publish or the preparation of the manuscript.

AUTHORS' CONTRIBUTIONS

X.Y.R., C.X.B. and B.C. designed the research. X.J.C., Q.L., Y.Y.C., L.X.W., and W.L.Z. conducted the experiments and analyzed the data. R.C.Y. and S.Y.Z. provide the bioinformatics analysis. X.Y.R., C.X.B., B.C., X.J.C., and C.W.C. provided the reagents. X.Y.R., C.X.B., B.C., and X.J.C. wrote the manuscript. All authors read and approved the final manuscript.

CONFLICT OF INTEREST

None declared.

DATA AVAILABILITY

Data will be made available on request.

APPENDIX A. SUPPLEMENTARY DATA

Supplementary data to this article can be found online at <https://doi.org/10.1016/j.molmet.2022.101600>.

REFERENCES

- Chai, A.W.Y., Lim, K.P., Cheong, S.C., 2020. Translational genomics and recent advances in oral squamous cell carcinoma. *Seminars in Cancer Biology* 61:71–83.
- Butler, L.M., Perone, Y., Dehairs, J., Lupien, L.E., de Laat, V., Talebi, A., et al., 2020. Lipids and cancer: emerging roles in pathogenesis, diagnosis and therapeutic intervention. *Advanced Drug Delivery Reviews* 159:245–293.
- Hoy, A.J., Nagarajan, S.R., Butler, L.M., 2021. Tumour fatty acid metabolism in the context of therapy resistance and obesity. *Nature Reviews Cancer* 21(12): 753–766.
- Hauck, A.K., Bernlohr, D.A., 2016. Oxidative stress and lipotoxicity. *The Journal of Lipid Research* 57(11):1976–1986.
- Zechner, R., Madeo, F., Kratky, D., 2017. Cytosolic lipolysis and lipophagy: two sides of the same coin. *Nature Reviews Molecular Cell Biology* 18(11):671–684.
- Pavlova, N.N., Zhu, J., Thompson, C.B., 2022. The hallmarks of cancer metabolism: still emerging. *Cell Metabolism* 34(3):355–377.
- Lian, J., Nelson, R., Lehner, R., 2018. Carboxylesterases in lipid metabolism: from mouse to human. *Protein Cell* 9(2):178–195.
- Li, Y., Zalzal, M., Jadhav, K., Xu, Y., Kasumov, T., Yin, L., et al., 2016. Carboxylesterase 2 prevents liver steatosis by modulating lipolysis, endoplasmic reticulum stress, and lipogenesis and is regulated by hepatocyte nuclear factor 4 alpha in mice. *Hepatology* 63(6):1860–1874.
- Ruby, M.A., Massart, J., Hunerdosse, D.M., Schonke, M., Correia, J.C., Louie, S.M., et al., 2017. Human carboxylesterase 2 reverses obesity-induced diacylglycerol accumulation and glucose intolerance. *Cell Reports* 18(3):636–646.
- Ren, X., Yang, X., Cheng, B., Chen, X., Zhang, T., He, Q., et al., 2017. HOPX hypermethylation promotes metastasis via activating SNAIL transcription in nasopharyngeal carcinoma. *Nature Communications* 8:14053.
- Wang, Y., Ren, X., Li, W., Cao, R., Liu, S., Jiang, L., et al., 2021. SPDEF suppresses head and neck squamous cell carcinoma progression by transcriptionally activating NR4A1. *International Journal of Oral Science* 13(1):33.
- Liu, Q., Luo, Y.W., Cao, R.Y., Pan, X., Chen, X.J., Zhang, S.Y., et al., 2020. Association between APOBEC3H-mediated demethylation and immune landscape in head and neck squamous carcinoma. *BioMed Research International* 2020:4612375.
- Zhang, L., Song, Y., Ling, Z., Li, Y., Ren, X., Yang, J., et al., 2019. R-spondin 2-LGR4 system regulates growth, migration and invasion, epithelial-mesenchymal transition and stem-like properties of tongue squamous cell carcinoma via Wnt/beta-catenin signaling. *EBioMedicine* 44:275–288.
- Ren, X.Y., Wen, X., Li, Y.Q., Zhang, J., He, Q.M., Yang, X.J., et al., 2018. TIPE3 hypermethylation correlates with worse prognosis and promotes tumor progression in nasopharyngeal carcinoma. *Journal of Experimental & Clinical Cancer Research* 37(1):227.
- Nagarajan, S.R., Butler, L.M., Hoy, A.J., 2021. The diversity and breadth of cancer cell fatty acid metabolism. *Cancer & Metabolism* 9(1):2.
- Sandoval, G., Herrera-Lopez, E.J., 2018. Lipase, phospholipase, and esterase biosensors (Review). *Methods in Molecular Biology* 1835:391–425.
- Qu, Q., Zeng, F., Liu, X., Wang, Q.J., Deng, F., 2016. Fatty acid oxidation and carnitine palmitoyltransferase I: emerging therapeutic targets in cancer. *Cell Death & Disease* 7:e2226.
- Cheng, X., Geng, F., Pan, M., Wu, X., Zhong, Y., Wang, C., et al., 2020. Targeting DGAT1 ameliorates glioblastoma by increasing fat catabolism and oxidative stress. *Cell Metabolism* 32(2):229–242 e228.
- Harayama, T., Riezman, H., 2018. Understanding the diversity of membrane lipid composition. *Nature Reviews Molecular Cell Biology* 19(5):281–296.
- Wang, B., Tontonoz, P., 2019. Phospholipid remodeling in physiology and disease. *Annual Review of Physiology* 81:165–188.
- Topham, M.K., 2006. Signaling roles of diacylglycerol kinases. *Journal of Cellular Biochemistry* 97(3):474–484.
- Gaud, C., Bebianna, C.S., Nguyen, A., Fedorova, M., Ni, Z., O'Donnell, V.B., et al., 2021. BioPAN: a web-based tool to explore mammalian lipidome metabolic pathways on LIPID MAPS. *F1000Research* 10:4.
- Pang, Z., Chong, J., Zhou, G., de Lima Morais, D.A., Chang, L., Barrette, M., et al., 2021. MetaboAnalyst 5.0: narrowing the gap between raw spectra and functional insights. *Nucleic Acids Research* 49(W1):W388–W396.

- [24] Kress, T.R., Sabo, A., Amati, B., 2015. MYC: connecting selective transcriptional control to global RNA production. *Nature Reviews Cancer* 15(10):593–607.
- [25] Yoon, H., Shaw, J.L., Haigis, M.C., Greka, A., 2021. Lipid metabolism in sickness and in health: emerging regulators of lipotoxicity. *Molecular Cell* 81(18):3708–3730.
- [26] Zhang, C., Zhu, N., Li, H., Gong, Y., Gu, J., Shi, Y., et al., 2022. New dawn for cancer cell death: emerging role of lipid metabolism. *Molecular Metabolism* 101529.
- [27] Goepfert, B., Renner, M., Singer, S., Albrecht, T., Zhang, Q., Mehrabi, A., et al., 2019. Prognostic impact of carboxylesterase 2 in cholangiocarcinoma. *Scientific Reports* 9(1):4338.
- [28] Capello, M., Lee, M., Wang, H., Babel, I., Katz, M.H., Fleming, J.B., et al., 2015. Carboxylesterase 2 as a determinant of response to irinotecan and neoadjuvant FOLFIRINOX therapy in pancreatic ductal adenocarcinoma. *Journal of the National Cancer Institute* 107(8):dju132.
- [29] Chen, Y., Capello, M., Rios Perez, M.V., Vykoukal, J.V., Roife, D., Kang, Y., et al., 2022. CES2 sustains HNF4alpha expression to promote pancreatic adenocarcinoma progression through an epoxide hydrolase-dependent regulatory loop. *Molecular Metabolism* 56:101426.
- [30] Uchida, K., Otake, K., Tanaka, K., Hashimoto, K., Saigusa, S., Matsushita, K., et al., 2013. Clinical implications of CES2 RNA expression in neuroblastoma. *Journal of Pediatric Surgery* 48(3):502–509.
- [31] Sanghani, S.P., Quinney, S.K., Fredenburg, T.B., Sun, Z., Davis, W.I., Murry, D.J., et al., 2003. Carboxylesterases expressed in human colon tumor tissue and their role in CPT-11 hydrolysis. *Clinical Cancer Research* 9(13):4983–4991.
- [32] Chalhoub, G., Kolleritsch, S., Maresch, L.K., Taschler, U., Pajed, L., Tilp, A., et al., 2021. Carboxylesterase 2 proteins are efficient diglyceride and mono-glyceride lipases possibly implicated in metabolic disease. *The Journal of Lipid Research* 62:100075.
- [33] Yuan, D., Wu, Z., Wang, Y., 2016. Evolution of the diacylglycerol lipases. *Progress in Lipid Research* 64:85–97.
- [34] Bilanges, B., Posor, Y., Vanhaesebroeck, B., 2019. PI3K isoforms in cell signalling and vesicle trafficking. *Nature Reviews Molecular Cell Biology* 20(9):515–534.